An Automated Over-the-Air Radiated Testing Platform for Reconfigurable Intelligent Surface

Yifa Li[1], Fengchun Zhang[1], Kim Olesen[1], Zhinong Ying[1], Gert Frølund Pedersen[1], Wei Fan[2,3]
[1]Antennas, Propagation and Millimeter-wave Systems Section,
Department of Electronic Systems, Aalborg University, Aalborg 9220, Denmark
E-mail: {yifal, fz, ko, zy, gfp}@es.aau.dk
[2]National Mobile Communications Research Laboratory,
School of Information Science and Engineering, Southeast University, Nanjing 210096, China
E-mail: weifan@seu.edu.cn
[3]Center for Wireless Communication-Radio Technology (CWC-RT),
Faculty of Information Technology and Electrical Engineering, Oulu University, Oulu 90570, Finland

***Abstract*—In the relentless quest to enhance wireless communication capabilities, reconfigurable intelligent surface (RIS) has emerged as a technology of immense promise. Armed with the beamforming capabilities, RIS can intelligently engineer and control wireless propagation environments. Consequently, an in-depth knowledge of RIS radiation characteristics has become important. This paper presents an automated over-the-air (OTA) radiated testing platform designed for characterizing RIS radiation. Operating in an anechoic chamber setup in a fully automated manner, the platform system utilizes multiple probes to expedite testing and employs a vector network analyzer (VNA) for testing signal measurement and recording. Controlled by a programmed controller, the system efficiently manages RIS operation with predefined code-book while the controller directs the system to conduct radiation measurements. To validate the designed testing platform system, RIS beam steering radiation measurements were conducted using a 2-bit 10×10 RIS. The measured results demonstrate the capabilities and reliability of the automated testing system.**

***Index Terms*—wireless communication, over-the-air (OTA) testing, reconfigurable intelligent surface (RIS), measurement.**

I. Introduction

The escalating demands driven by 5G and the forthcoming requirements of 6G wireless communication have triggered investigations into higher-frequency transmission signals. These signals provide expanded bandwidth and unlock the potential for elevated data rates [1], [2]. Nonetheless, this higher-frequency domain poses inherent hurdles, characterized by substantial propagation losses and diminished coverage [3]. In response to these challenges, RIS emerges as a transformative technology poised to enhance wireless communication system performance [4].

By harnessing metamaterial-based phase shifters, RIS devices can manipulate the phase of reflected electromagnetic signals, enabling adaptive beamforming that steers these signals in specific directions [5]. This optimization substantially bolsters signal strength, leading to significant improvements in wireless communication performance. In [6], RIS technology was applied in tandem with a compressive sensing-based beamforming algorithm, dynamically directing and concentrating signals toward the intended receiver location. Real-world experiments showcased substantial performance improvements, including reduced Bit Error Rate (BER) and enhanced Signal-to-Noise Ratio (SNR). In [7], a downlink multi-user system was facilitated by an RIS that redirects signals from the base station (BS) toward the users, and a hybrid beamforming scheme was proposed. Theoretical analysis and numerical simulations demonstrate that effective sum-rate performance can be achieved in RIS-based systems with an appropriate sized RIS and a limited number of discrete phase shifts.

Furthermore, efficient beamforming design is a crucial component in RIS-aided joint localization and synchronization. In [8], the strategic beamforming optimization significantly enhances the performance of both localization and synchronization processes, ensuring optimal outcomes. To ensure RIS systems' real-world viability, it's essential to comprehensively measure and characterize RIS radiation. These measurements validate practical applicability and offer crucial insights for refining designs and advancing RIS-enabled wireless communication systems. While there have been significant efforts to measure mmWave phased array radiation for laboratory assessment [9]–[11], the specific domain of RIS radiation measurement has received limited attention.

In [12], a designed 2-bit RIS operating at a frequency of 2.3 GHz was evaluated within a compact anechoic chamber. The experiment confirmed the wide-range beam-scanning capabilities of the RIS, based on the measured radiation patterns. In [13], a matching pursuit algorithm was used to estimate the wireless channel of the RIS-aided wireless system. The effectiveness of this approach in beam steering was verified through measurements of the RIS radiation patterns. Unlike conventional phased arrays that transmit signals from the RF port, RIS operates by reflecting signals from the radio propagation environment. This characteristic makes it incompatible with conventional phased array radiated testing systems. Additionally, the substantial number of elements in RIS highlights

978-88-31299-09-1/24/$31.00 ©2024 IEEE

the need for an automated experimental platform to expedite measurements and ensure high-quality measurement results.

This paper focuses on this fundamental work, presenting an automated OTA radiated testing platform designed for measuring RIS radiation. The proposed testing platform can be used as a reference for solutions in the field of RIS radiation measurements. The detailed measurement campaign and characterization of RIS beamforming presented and served as a validation of this testing platform. Firstly, RIS beamforming theory is provided in Section II. Subsequently, Section III showcases the testing platform and RIS beamforming measurement campaign, and the measurement results are then analyzed. Finally, the conclusion is offered in Section IV.

II. Basic Theory of RIS Beamforming

To improve communication in a wireless system with RIS, effective RIS-based beamforming is crucial. It optimizes signal reception from the transmitter and directs signals efficiently to the receiver, enhancing communication quality by delivering a high-power signal. Precise control of RIS element phase shifts is essential, relying on accurate knowledge of transmitter and receiver positions / directions.

The configuration of the wireless communication system aided by RIS comprises certain fundamental geometric parameters, illustrated in Fig. 1. In the scenario, assumed that the Tx is positioned in the near-field of the RIS, while the Rx is situated in the far-field of the RIS. Specifically, with the Tx in the near-field of the RIS, the transmitted signal from the Tx takes the form of a spherical wavefront that propagates towards the RIS. Consequently, the phase distribution of the signal received by the RIS element can be expressed as follows:

$$\alpha_n = -\frac{2\pi}{\lambda} d_n, \tag{1}$$

where λ represents the wavelength of the transmitted signal and d_n stands for the distance between the center of the Tx and the n-th element of the RIS. To achieve maximum signal reception, it is essential to compensate for the phase distribution $\{\alpha_n\}$. Therefore, the phase shifts applied to the RIS elements for receiving the signal can be expressed as follows:

$$\beta_n = -\alpha_n, \tag{2}$$

As the Rx is located in the far-field of the RIS, incident plane waves are reflected from the RIS towards the Rx. To ensure that the RIS effectively performs beamforming, with the main beam precisely directed towards the Rx, the phase shifts applied to the RIS elements for reflecting these signals. can be expressed as

$$\gamma_n = -\frac{2\pi}{\lambda} \vec{r}_n \hat{r}_0 = -\frac{2\pi}{\lambda} \sin\theta_0 (x_n \cos\varphi_0 + y_n \sin\varphi_0), \tag{3}$$

Where $\vec{r}_n$ represents the position vector of the n-th RIS element, and $\hat{r}_0$ denotes the direction vector from the RIS to the Rx. Additionally, θ_0 represents the elevation angle, and φ_0 denotes the azimuth angle. Consequently, the total phase shift introduced by each RIS element, which is essential for receiving signals from the Tx and subsequently reflecting them towards the Rx with beamforming functionality, can be expressed as:

$$\phi_n = \alpha_n + \gamma_n + \delta_0, \tag{4}$$

where (φ_0, θ_0) is the RIS beamforming direction, and (x_n, y_n) is the coordinate of the n-th RIS element in the system. Moreover, δ_0 is a constant phase, illustrating that a relative phase shift is applied in the element for RIS beamforming. Additionally, if the Tx is located at the far-filed of RIS, the phase distribution α_n of the signal received by the RIS element can be calculated with reference to Eq. (3).

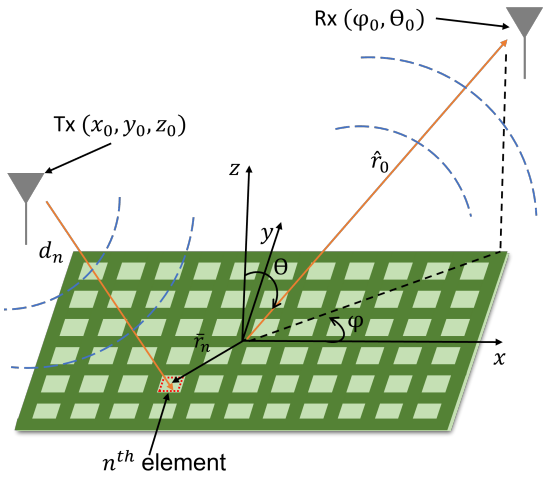

Fig. 1: The general geometrical parameters of a RIS aided wireless communication system, where assumed that the Tx is positioned in the near-field of the RIS and the Rx is situated in the far-field of the RIS.

III. Automated OTA Radiated Testing Platform

A. Testing Platform

The automated OTA radiated testing platform for RIS is built in an anechoic chamber equipped with a turntable and a probe ring containing multiple antennas, as shown in Fig. 2. The RIS to be measured, positioned on the turntable, was subject to rotation. A plastic structure held the feeding antenna in close proximity to the RIS within its near-field. Key components of the testing platform system are introduced below:

1) The measured RIS, detailed in Table I, comprises a 10×10 element panel with a rectangular layout operating within the 3.4 $\sim$ 3.6 GHz frequency range. Each RIS element features a 2-bit resolution phase-shifter, providing tunable phase shifts of 0°, 90°, 180°, and 270°. The phase-shifting functionality is achieved through PIN diode circuit control, managed by an FPGA-based control circuit board. The phase shift accuracy is maintained within 90° ± 15°.
2) The VNA operated at 3.5 GHz, utilizing a 100 Hz Intermediate Frequency (IF) bandwidth and -10 dBm

TABLE I: RIS Specification

Characteristic	Value
Model	Actenna I24−S35
Array size	10×10 elements
Module size	430 mm (W)×430 mm (H)
Operation frequency	3.4−3.6 GHz
Phase-shifter resolution	2-bit
Phase-shifter accuracy	90°±15°
Polarization	Orthogonal dual linear polarization
Communication protocol	Serial Communication

transmitting power. Transmission coefficients between the feeding antenna and chamber probes were recorded during the measurements.

3) The feeding antenna transmits signals to the RIS, located 50 cm away from the RIS surface center. Additionally, The feeding antenna is positioned at an azimuth angle of 0° and an elevation angle of 50° relative to the RIS surface center.
4) The multiple chamber probe antennas are integrated into a ring structure and serve as the receiving antennas within the measurement system. A switch system is connected to the probe antennas, allowing it to change the operational status of the probe antennas.
5) The controller employs universal asynchronous receiver-transmitter (UART) serial communication to transmit the phase shift code-book to the RIS under measurement. This code-book, represented as an $M \times N$ matrix, associates specific phase shift values with individual elements of the $M \times N$ RIS, thereby controlling the radiation characteristics of the RIS. Additionally, the controller manages the switch system to activate or deactivate the probe antennas. The VNA is also under the controller's command, recording the testing signal. Through the efficient switching of probe antennas and precise control rotation of the turntable in azimuth and elevation, the 3D radiation pattern of the measured RIS can be retrieved. The resolution of the radiation measurement can be adjusted by configuring the rotation step of the turntable.

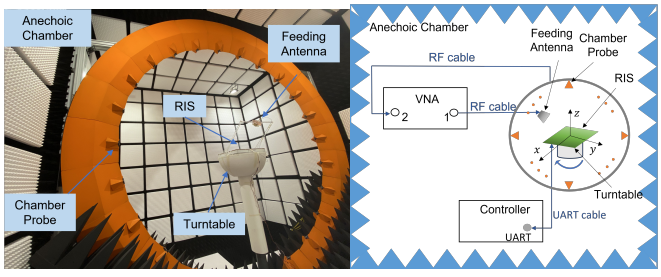

(a) (b)

Fig. 2: The photograph (a) and the diagram (b) of the automatic OTA radiated testing platform for RIS.

B. Testing Campaign

In this context, the RIS beamforming radiation pattern measurements serve as an illustrative example to demonstrate the measurement procedure and validate the capability of the testing platform system. As detailed in Section II, the beamforming phase shift $\{\phi_n\}$ of RIS elements comprises two components: the phase shift $\{\alpha_n\}$ for receiving signals and the phase shift $\{\gamma_n\}$ for reflecting signals. Initially, to measure the RIS's beamforming radiation, a selected beamforming direction (φ_0, θ_0) of (0°, 30°) was selected. Fig. 3 illustrates the calculated values of $\{\alpha_n\}$ and $\{\gamma_n\}$ for this configuration.

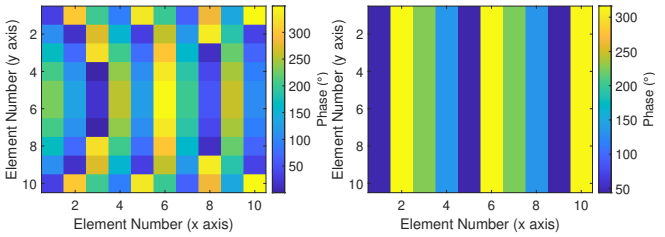

(a) (b)

Fig. 3: The beamforming phase shift of RIS elements for receiving signal (a) and reflecting signal (b), with a beamforming direction set at (0°, 30°).

Following, the total beamforming phase shift setting of RIS elements is obtained as shown in Fig. 4 (a). Notably, the measured RIS employs a 2-bit phase shift resolution. Consequently, a method to convert the calculated phase shift into the RIS's tunable phase shift was applied. This method is detailed as follows:

$$f(\Phi_n) = \begin{cases} 0°, & \text{if } \Phi_n \text{ is closest to } 0° \\ 90°, & \text{if } \Phi_n \text{ is closest to } 90° \\ 180°, & \text{if } \Phi_n \text{ is closest to } 180° \\ 270°, & \text{if } \Phi_n \text{ is closest to } 270° \end{cases} \tag{5}$$

Finally, the beamforming code-book for setting phase shift in RIS element to perform beamforming with the direction of (0°, 30°) as shown in Fig. 4 (b). Moreover, to validate the beam steering capability of RIS in both azimuth and elevation, the beamforming of direction (φ_0, θ_0) = (225°,45°) was selected for measurement. The calculated beamforming phase shift and the beamforming code-book of RIS elements as illustrated in Fig. 5.

After calculating the phase shift settings of the RIS elements and converting them into a cood-book, the controller transmits the code-book to the RIS during the measurement phase. The RIS then receives and interprets the code-book, adjusting the phase shift of each element based on the values specified in the code-book. Following the phase shift adjustments of RIS elements, the controller initiates the activation of probe antennas positioned at different elevation angles with the

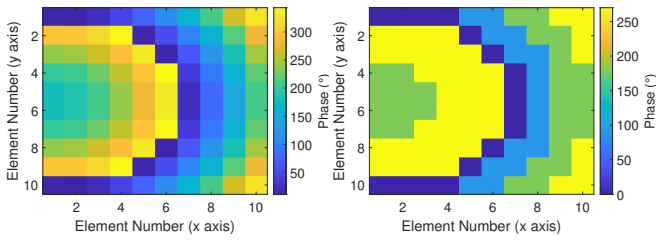

(a) (b)

Fig. 4: The total beamforming phase shift of RIS elements (a) and the converted beamforming code-book (b) to perform beamforming with the direction of (0°, 30°).

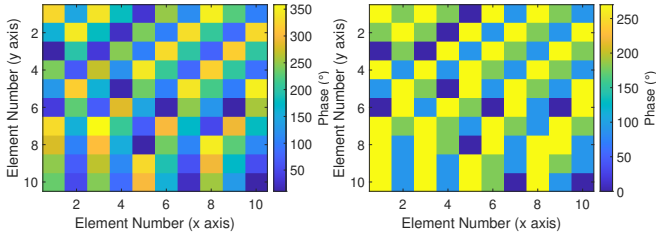

(a) (b)

Fig. 5: The total beamforming phase shift of RIS elements (a) and the converted beamforming code-book (b) to perform beamforming with the direction of (225°, 45°).

switch system. Concurrently, a VNA begins recording the transmission coefficients between the feeding antenna and the activated probe antenna.

The switch operation responsible for probe antenna activation is electrically driven, resulting in rapid switching time. As a result, the measurement process of on elevation cut of RIS radiation occurs swiftly. Upon completion of a single elevation cut measurement, the turntable is rotated one step at a predetermined angle. This turntable rotation enables the measurement of a new elevation cut of RIS radiation. The probe antenna switching and turntable rotating process repeat iteratively until the system has completed scanning all the elevation cuts, generating a comprehensive 3D pattern scan of the RIS radiation. Importantly, the entire measurement process is automated, enhancing its efficiency and reliability.

C. Testing Results

The measured 2-bit RIS beamforming pattern, targeted at (φ_0, θ_0) = (0°,30°), exhibits a symmetric main lobe with peak gain at (6°,30°), as shown in Fig. 5. Despite a 6° azimuthal error, this deviation in 3D space is minimal, showcasing effective beamforming. The main beam has a narrow beamwidth of 15.0°, which highlights the ability of the RIS to concentrate radiation in a specific direction. Additionally, there are some side lobes that are typical in phased array beamforming patterns, and it is not straightforward to apply advanced beamforming algorithms to suppress these side lobes due to the limited phase shift resolution on RIS. The peak gain of the receiver beam is 12.0 dB. The gain of the RIS beamforming will increase as the size of the RIS increases, and high gain is critical for long-range wireless communications and radar applications. Notably, the area around direction (φ_0, θ_0) = (0°,90°) exhibits higher power possibly due to the line-of-sight path or diffraction path exists between the feeding antenna and the chamber probe in the vicinity of (φ_0, θ_0) = (0°,90°). The measured RIS is not large enough to block all the direct propagation paths between the feeding antenna and probe. The measured beamforming radiation at beamforming direction (φ_0, θ_0) = (225°,45°) as shown in Fig. 6. There also is a main beam directs to the intended angle and the angle, beamwidth, peak gain of the main beam are (39°,222°), 18° and 8.7 dB, respectively.

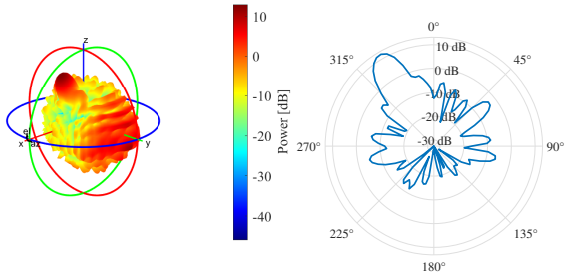

(a) (b)

Fig. 6: The measured 2-bit 10×10 RIS beamforming radiation in the beamforming direction (φ_0, θ_0) = (0°,30°), 3D pattern (a) and 2D cut pattern with azimuth angle of 0° (b).

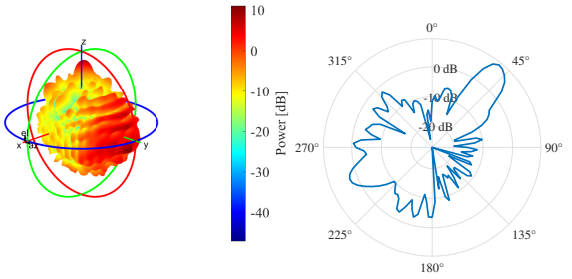

(a) (b)

Fig. 7: The measured 2-bit 10×10 RIS beamforming radiation in the beamforming direction (φ_0, θ_0) = (225°,45°), 3D pattern (a) and 2D cut pattern with azimuth angle of 45° (b).

Furthermore, we conducted measurements of RIS beam scanning at two different cuts with azimuth angles, 0° and 45°, as depicted in Fig. 7 and Fig. 8, respectively. The desired beamforming directions are indicated in the figure legends. These measurements confirm that the actual beamforming directions closely align with the intended ones, showcasing the RIS's capacity for effective beamforming adjustments. This capability allows the RIS to intelligently control the phase of reflected electromagnetic waves, enabling precise

energy focusing in user-specified directions, thereby reducing signal dispersion and interference and enhancing connection reliability.

However, an observed beamforming performance deterioration occurs as the elevation angle of beamforming increases. As the beamforming elevation angle increases, the main beam direction error increases, the main beam width widens, and the peak gain of the main beam decreases. This phenomenon results from multiple contributing factors. A major factor is that the larger the beamforming elevation angle, the smaller the effective aperture of the RIS. As the beamforming elevation angle increases, the physical area available for signal capture decreases, impacting the RIS's energy concentration ability. In addition, the limited adjustable phase shift capability and inherent control errors of the RIS element also affect accurate beam steering.

In summary, the RIS beamforming radiation measurements validate this automated OTA testing platform. The measured results align with theoretical expectations, confirming the platform's capability.

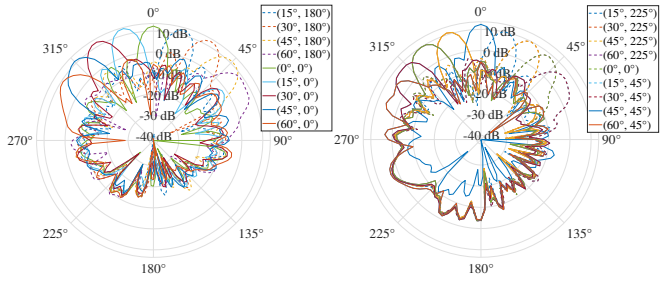

(a) (b)

Fig. 8: The measured RIS beam scanning radiation pattern in two cuts with azimuth angle of 0° (a) and 45° (b). The directions of multiple intended beamforming in each cut as shown in the legend of the figure.

IV. Conclusion

This paper introduces an automated OTA radiated testing platform tailored for RIS. Using a practical demonstration involving a 2-bit 10×10 RIS, the platform is employed to conduct beamforming radiation measurements and characterizations. The results showcase RIS's ability to effectively facilitate beam steering, holding promise for improved wireless communication services. However, performance limitations become apparent, especially at higher elevation angles during beamforming, warranting further research and optimization. The close agreement between measured and theoretical RIS beamforming radiation patterns validates the testing platform's capabilities. Furthermore, this versatile platform can potentially perform tasks such as diagnosing RIS element status, evaluating beamforming performance, and validating RIS-assisted wireless communication systems in the future.

Acknowledgments

The authors would like to thank Kristian Bank for his assistance in measuring campaigns and Sony for the RIS device and antennas in the experiments. This research is supported by HORIZON-JU-SNS-2022-STREAM-B-01-03 6G-SHINE project (Grant Agreement No. 101095738).

References

[1] S. Chen, Y.-C. Liang, S. Sun, S. Kang, W. Cheng, and M. Peng, "Vision, requirements, and technology trend of 6g: How to tackle the challenges of system coverage, capacity, user data-rate and movement speed," IEEE Wireless Communications, vol. 27, no. 2, pp. 218–228, 2020.

[2] M. Alsabah, M. A. Naser, B. M. Mahmmod, S. H. Abdulhussain, M. R. Eissa, A. Al-Baidhani, N. K. Noordin, S. M. Sait, K. A. Al-Utaibi, and F. Hashim, "6g wireless communications networks: A comprehensive survey," IEEE Access, vol. 9, pp. 148 191–148 243, 2021.

[3] A. N. Uwaechia and N. M. Mahyuddin, "A comprehensive survey on millimeter wave communications for fifth-generation wireless networks: Feasibility and challenges," IEEE Access, vol. 8, pp. 62 367–62 414, 2020.

[4] Y. Liu, X. Liu, X. Mu, T. Hou, J. Xu, M. Di Renzo, and N. Al-Dhahir, "Reconfigurable intelligent surfaces: Principles and opportunities," IEEE Communications Surveys Tutorials, vol. 23, no. 3, pp. 1546–1577, 2021.

[5] C. Pan, H. Ren, K. Wang, J. F. Kolb, M. Elkashlan, M. Chen, M. Di Renzo, Y. Hao, J. Wang, A. L. Swindlehurst, X. You, and L. Hanzo, "Reconfigurable intelligent surfaces for 6g systems: Principles, applications, and research directions," IEEE Communications Magazine, vol. 59, no. 6, pp. 14–20, 2021.

[6] M. M. Amri, N. M. Tran, and K. W. Choi, "Reconfigurable intelligent surface-aided wireless communications: Adaptive beamforming and experimental validations," IEEE Access, vol. 9, pp. 147 442–147 457, 2021.

[7] B. Di, H. Zhang, L. Song, Y. Li, Z. Han, and H. V. Poor, "Hybrid beamforming for reconfigurable intelligent surface based multi-user communications: Achievable rates with limited discrete phase shifts," IEEE Journal on Selected Areas in Communications, vol. 38, no. 8, pp. 1809–1822, 2020.

[8] A. Fascista, M. F. Keskin, A. Coluccia, H. Wymeersch, and G. Seco-Granados, "Ris-aided joint localization and synchronization with a single-antenna receiver: Beamforming design and low-complexity estimation," IEEE Journal of Selected Topics in Signal Processing, vol. 16, no. 5, pp. 1141–1156, 2022.

[9] W. Fan, P. Kyosti, M. Rumney, X. Chen, and G. F. Pedersen, "Over-the-air radiated testing of millimeter-wave beam-steerable devices in a cost-effective measurement setup," IEEE Communications Magazine, vol. 56, no. 7, pp. 64–71, 2018.

[10] P. Kyösti, W. Fan, G. F. Pedersen, and M. Latva-Aho, "On dimensions of ota setups for massive mimo base stations radiated testing," IEEE Access, vol. 4, pp. 5971–5981, 2016.

[11] H. Gao, F. Zhang, G. F. Pedersen, and W. Fan, "A fast multibeam measurement method for millimeter-wave phased arrays," IEEE Antennas and Wireless Propagation Letters, vol. 21, no. 7, pp. 1502–1506, 2022.

[12] L. Dai, B. Wang, M. Wang, X. Yang, J. Tan, S. Bi, S. Xu, F. Yang, Z. Chen, M. D. Renzo, C.-B. Chae, and L. Hanzo, "Reconfigurable intelligent surface-based wireless communications: Antenna design, prototyping, and experimental results," IEEE Access, vol. 8, pp. 45 913–45 923, 2020.

[13] M. M. Amri, N. M. Tran, and K. W. Choi, "Reconfigurable intelligent surface-aided wireless communications: Adaptive beamforming and experimental validations," IEEE Access, vol. 9, pp. 147 442–147 457, 2021.